15th Australasian Fluid Mechanics Conference
The University of Sydney, Sydney, Australia
13-17 December 2004

Active Flow Control over a NACA 0015 Airfoil using a ZNMF Jet

A. Tuck and J. Soria

Laboratory for Turbulence Research in Aerospace and Combustion (LTRAC)
Department of Mechanical Engineering, Monash University, Melbourne, AUSTRALIA 3800

Abstract

The effect of using a wall-normal, zero-net-mass-flux (ZNMF) jet located at the leading edge of a NACA 0015 airfoil as an active flow control device was investigated. Experiments were conducted over a two-dimensional airfoil in a water tunnel at a Reynolds number of 3.08×10^4 for parametric investigations and particle image velocimetry (PIV) and at a Reynolds number of 1.54×10^4 for flow visualisations. The largest lift increases were observed when a non-dimensional frequency of 1.3 and an oscillatory momentum blowing coefficient of 0.14% were employed. Under these forcing conditions the stall angle of the airfoil was mitigated from an angle of attack of 10^o to an angle of attack of 18^o, resulting in a maximum lift coefficient increase of 46% above the uncontrolled lift coefficient. Planar laser induced fluoroscopy (PLIF) and PIV revealed that the lift increments were the result of the generation of a train of large-scale, spanwise lifting vortices that convected over the suction surface of the airfoil. The presence of these structures resulted in the flow seemingly remaining attached to the upper surface of the airfoil for a wider range of angles of attack.

Introduction

Flow control over airfoils is primarily directed at increasing the lift and decreasing the drag produced by the airfoil. This is usually achieved by manipulating the boundary and shear layer flows in order to minimise the separation region over the suction surface of the airfoil. Active flow control refers to the process of expending energy in order to modify the flow [2]. This is distinct from passive techniques where flow control is provided without expending energy through means such as geometric shaping. One of the main advantages of active, rather than passive, flow control is that the control device can be switched on and off when required.

Many techniques for implementing active flow control have been proposed previously. These include: piezoelectric devices, vibrating flaperons, oscillating wires, boundary layer suction and blowing devices and the ZNMF jet that was studied here. A ZNMF jet 'transfers linear momentum to the flow system without net mass injection across the system boundary' [7]. ZNMF jets are commonly formed using a sinusoidally oscillating membrane to alternatively force fluid through an orifice into the external flow field and entrain fluid back through the orifice. During the forcing stroke the ejected fluid separates at the sharp edges of the orifice, forming a shear layer that rolls up to form a vortex ring for the case of a round synthetic jet or a vortex pair for the case of a plane synthetic jet. By the time the membrane begins its intake stroke, the vortex pair is 'sufficiently distant from the orifice that it is virtually unaffected by the entrainment of fluid into the cavity' [3,7].

The flow around an airfoil actively controlled by a ZNMF jet can be characterised using the following non-dimensional groups. Firstly, the non-dimensionalised excitation frequency is defined as:

$$F^+ \equiv \frac{fc}{U_\infty} \tag{1}$$

Where c is the chord length of the airfoil and f is the excitation frequency. The second parameter of significance is the oscillatory momentum blowing coefficient; a measure of the momentum imparted on the flow field by the ZNMF jet normalised by a characteristic momentum for the unexcited flow field, namely:

$$c_\mu \equiv 2\frac{h}{c}\left(\frac{u_{j\ rms}}{U_\infty}\right)^2 \tag{2}$$

Where h is the height of the slot and $u_{j\ rms}$ is the rms velocity of the jet in the exit plane. An alternative measure of the strength of the ZNMF jet is the velocity ratio, defined as:

$$VR \equiv \frac{u_{j\ rms}}{U_\infty} \tag{3}$$

The use of ZNMF jets as an active flow control device has been shown in a number of studies to effectively delay the stall angle of an airfoil [1,2,4,5]. In delaying the stall angle the maximum lift coefficient produced by the airfoil is invariably increased. The power required to produce equivalent increases in the lift coefficient have been found to be approximately an order of magnitude lower for oscillatory control rather than for steady blowing techniques [5]. It has been reported that the actively controlled flow field shows little dependence on Reynolds number, except in the case where laminar-turbulent transition effects are significant [6]. Studies where the control actuators were placed closest to the separation point have reported the most beneficial results. The magnitude of the jet momentums found to be most effective has been varied, owing primarily to differences in the location and application of the control. Optimal results have generally been found when excitation at non-dimensional frequencies in the range of 0.58-2 was employed [2,5]. However, other researchers have had success operating at non-dimensional frequencies an order of magnitude higher.

The motivation for the work presented in this paper was to determine the most effective excitation parameters for increasing the post-stall lift produced by the particular airfoil geometry employed, and to characterise the flow structure around the controlled airfoil when these optimum excitation parameters were applied.

Experimental Apparatus and Method

A re-circulating water tunnel, having a 5m long test section with a cross sectional area of 500mm x 500mm was used in this investigation. Water was used as the working fluid in these experiments as by virtue of its lower kinematic viscosity when compared to air, velocities (and hence characteristic frequencies) a factor 18 lower are inherent for the same Reynolds number flows. This affords for much more relaxed acquisition and excitation timescales.

All experiments were conducted using a Perspex NACA 0015 airfoil with a chord length of 100mm and a span of 510mm. The airfoil was mounted vertically in the test section of the water tunnel such that the base of the airfoil maintained a slight

clearance (2-5mm) with the base of the water tunnel. In this configuration the top of the airfoil protruded above the free surface of the working fluid at all times. This arrangement ensured that the flow-field around the airfoil was ideally free from 3-Dimensional effects due to the generation of tip vortices.

A slot of height 0.15mm, oriented normal to the surface at the leading edge, extended the entire span of the airfoil. This slot intersected a 5mm diameter hole through which pressure oscillations were supplied to generate the ZNMF jet, as shown in figure 1. The relative slot height of $^{h}/_{c}$ = 0.15% used in this investigation was smaller than those used in previous research. The slot height was minimised in order to maximise the jet exit velocity for the same displacement of fluid, as it was postulated that the control would be more effective for higher jet exit velocities.

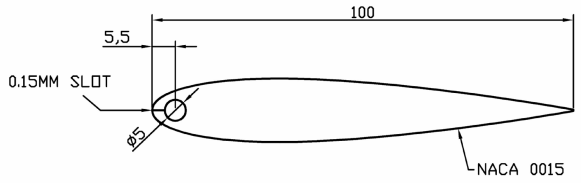

Figure 1. Cross-sectional view of the NACA 0015 airfoil tested (all dimensions in mm).

The pressure oscillations were supplied by a 20mm diameter piston/cylinder arrangement that was driven by a computer-controlled stepper motor via a Scotch-Yoke mechanism. The frequency of the pressure oscillations was controllable by altering the rotational speed of the stepper motor, whilst the magnitude of the oscillations was adjusted by varying the crank length of the Scotch-Yoke mechanism.

The airfoil was mounted on a force transducer, which allowed the lift and drag forces acting on the airfoil to be measured with a resolution of 0.1N. All force measurements reported have been averaged over 500 samples obtained from the force sensor. In order to isolate the fluidic forces from the external forces acting on the airfoil (for example forces arising from the nylon hose connection between the airfoil and the excitation system) force measurements collected with a stationary free stream were subtracted from the dynamic test results.

The zero degree angle of attack position of the airfoil was defined as being the angle for which the measured lift force for the uncontrolled airfoil was zero. As the airfoil used was symmetric, this condition corresponded to the airfoil being aligned with the freestream.

The structure of the flow field was examined by introducing a small amount of Kiton Red 620 fluorescent dye into the ZNMF jet cavity. This dye was ejected from the jet orifice into the external flow during the expulsion phase of the excitation cycle. An Nd:YAG laser sheet, incident on the mid-plane of the airfoil, resulted in fluorescence of the dye. The addition of a constant mass flow of dye to the jet violated the zero-net-mass-flux condition imposed, however it was assumed that the mass of the additional fluid was negligible relative to the total mass flux through the jet orifice during the excitation period. Instantaneous, randomly averaged and phase averaged images of the flow structure were captured using a monochrome digital camera with a CCD array size of 1280 x 1024 pixels.

For the PIV investigation the tunnel was seeded with 11µm hollow glass spheres. An identical laser and camera configuration to that used for the PLIF study was used in this phase of the investigation. The resulting PIV image pairs had a spatial resolution, $^{\Delta}/_{c}$, of 0.075%. These image pairs were analysed using a multi-grid cross-correlation digital PIV algorithm. For more details of the algorithm used refer to [8]. Each image pair was segregated into interrogation windows with a characteristic dimension of 1.2%c, which resulted in a 64 x 80 vector field being obtained for each realisation of the flow. 50 velocity fields were computed and averaged for every flow configuration investigated. Velocity fields were obtained for a plane immediately surrounding the airfoil and a plane exactly one image plane width downstream of the initial plane. Following processing, these velocity fields were patched together to form a vector field of twice the original aspect ratio.

Results and Discussion

Parametric Study

The dependence of the effectiveness of the control on the excitation frequency was evaluated by maintaining a constant jet momentum and varying the excitation frequency at a post-stall angle of attack of 18°. A relatively broad range of forcing frequencies between F^+ = 0.6 and F^+ = 1.4 were effective in enhancing the post-stall lift coefficient. The optimal forcing frequencies were determined to be a pair of frequencies symmetrically offset from a non-dimensional frequency of unity at F^+ = 0.7 and F^+ = 1.3.

The effect of varying the jet momentum at an angle of attack of 18° for both of the optimum excitation frequencies identified above appears in figure 2. For both frequencies the lift coefficient increase was approximately proportional to the square root of the jet momentum, and hence linearly proportional to the jet velocity ratio. A peak was found in the effectiveness of the active control for F^+ = 1.3 at a jet momentum corresponding to c_μ = 0.14% (VR = 0.65). No such peak was observed for an excitation frequency of F^+ = 0.7 in the range of jet momentums investigated. A possible explanation for the presence of such a peak is that at c_μ = 0.14% the maximum reattachment effect was realised from the ZNMF jet. Above this momentum the velocity of the jet may have been large enough to force the boundary layer to separate locally, resulting in the loss of lift demonstrated in figure 2.

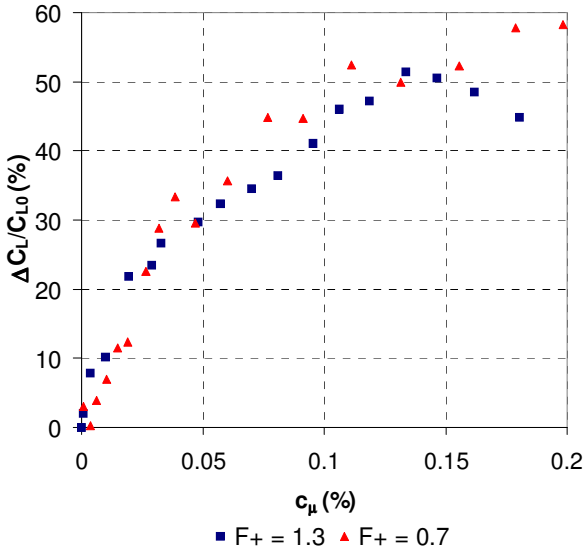

Figure 2. Percentage lift increment above the uncontrolled case for various jet momentums at α = 18°.

The optimum forcing parameters employed throughout the remainder of the investigation were defined as F^+ = 1.3 and c_μ = 0.14%, despite the fact that sightly greater lift gains were noted for F^+ = 0.7 than for F^+ = 1.3. This was due to the fact that the lift increments were found to be less repeatable, especially at

lower Reynolds numbers, if the lower effective forcing frequency were employed. Good repeatability was however found for F^+ = 1.3, hence its use as the optimum excitation frequency.

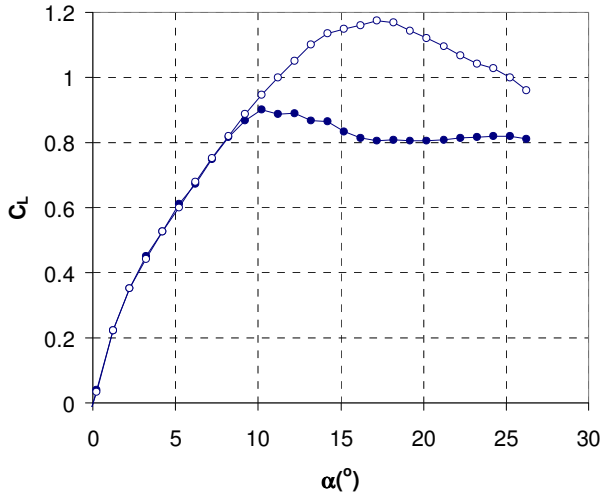

Figure 3. Controlled (F^+=1.3, c_μ=0.14%) airfoil (open circles) and uncontrolled airfoil (closed circles) lift coefficients.

The optimally controlled and the uncontrolled lift curves are presented in figure 3. Activation of the control is noted to result in the stall angle of the airfoil being mitigated from an angle of attack of 10° up to an angle of attack of 18°. Under these controlling parameters a maximum lift coefficient increase of 46% above the uncontrolled lift coefficient is observed at an angle of attack of 18°. The drag force acting on the airfoil was also significantly reduced for angles of attack between 10° and 18°. Significant lift increments were noted throughout the post-stall region investigated, however for angles of attack less than the uncontrolled airfoil stall angle no lift enhancement was realisable by activation of the control. Hence, it was concluded that the control must work by affecting the separated shear layer dynamics.

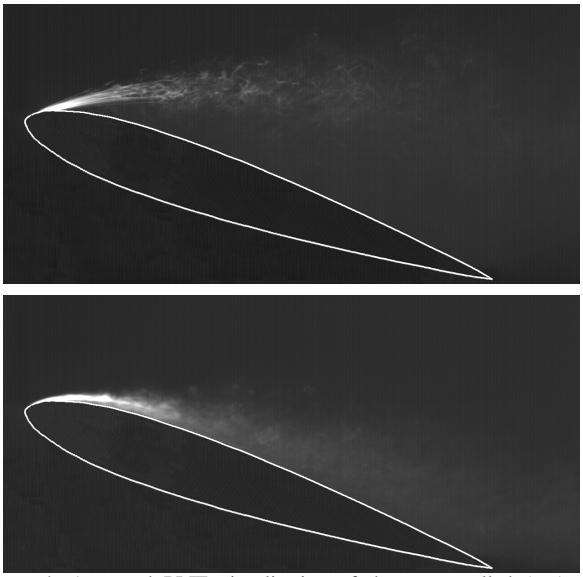

Figure 4. Averaged PLIF visualisation of the uncontrolled (top) and controlled (bottom) airfoils at α = 18°.

Flow Characterisation

Flow characterisation was undertaken at α = 18°, as the lift and drag measurements suggested the greatest difference between the uncontrolled and the controlled flow fields at this angle of attack. It must however be noted that at an angle of attack of 18° the adverse pressure gradient on the suction surface of the airfoil is such that the excitation is on the verge of losing effectiveness in controlling the flow.

The PLIF images shown in figure 4 demonstrate that the boundary layer of the uncontrolled airfoil has separated right at the leading edge to form a clearly defined separated shear layer that is unable to overcome the adverse pressure gradient required for reattachment to occur. From the trajectory of the separated shear layer it can be inferred that a massive separation region exists above the uncontrolled airfoil at this angle of attack. In contrast, the flow appears to be attached over the entire length of the suction surface of the controlled airfoil.

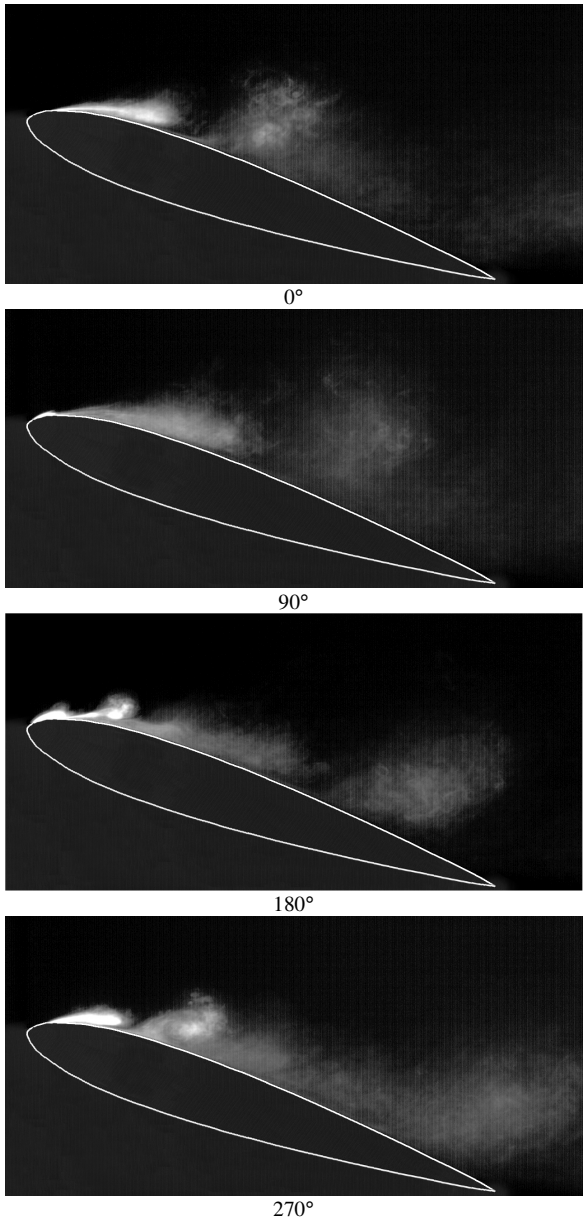

Figure 5. Phase averaged visualisations of the controlled airfoil

Examination of the phase averaged PLIF visualisations of the controlled airfoil presented in figure 5 reveals that the generation of a train of large, spanwise, coherent structures was responsible for the apparent reattachment of the flow. In these images 0° phase is defined as the point in the excitation cycle where fluid begins to be expelled from the jet orifice. The fluid ejected from the ZNMF jet orifice is first observed in the external flow field at a phase angle of 90°. At a phase angle of 180° the presence of multiple vortices is just discernable in the image. Between a phase of 180° and a phase of 270° these smaller vortices are observed to coalesce to form a single, larger, more intense

vortex. It is suspected that a vortex pairing event, or a series of vortex pairing events, that resulted in the formation of the larger vortex occurred in between these two phase angles. By virtue of its larger size, the core of the resulting single vortex is offset a significant distance further from the surface than those of the multiple, smaller vortices.

For the forcing frequency used in figure 5, F^+ = 1.3, the structures required almost two entire excitation periods to convect from their origin at the leading edge to the trailing edge. This translates to two structures residing over the suction surface of the airfoil at any time; one from the current excitation period that exists over the forward half of the airfoil and one generated during the previous excitation period that is evident over the aft portion of the airfoil. In contrast, for the lower effective forcing frequency, F^+ = 0.7, the vortices generated required just one excitation period to convect over the same distance.

Streamlines were determined from the PIV results by integrating across the velocity vector field from the inflow conditions. Figure 6 shows phase averaged streamlines for the controlled airfoil at a phase angle of 180°. It is apparent from the streamlines presented that the vortices generated over the upper surface of the airfoil are of negative sign. Being of the same sign as the lifting vortex, the vortex is able to 'roll' over the surface of the airfoil. It is postulated that this rolling motion is what allowed the vortex to move away from the leading edge at a faster rate than the bulk of the fluid ejected from the leading edge orifice - a phenomenon that was noted in the PLIF visualisations displayed in figure 5.

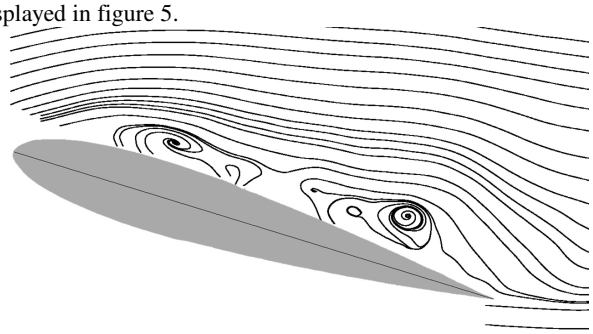

Figure 6 – Phase averaged streamlines around the controlled airfoil for a phase angle of 180°.

Only negative sign vortices were ever observed over the suction surface of the airfoil, however a vortex pair consisting of both a positive and a negative sign vortex is created when the flow separates at the sharp edges of a planar ZNMF jet orifice. The explanation offered for this behaviour is that the positive half of the vortex pair is annihilated by superposition of vorticity of a negative sign, which is inherent in the boundary and shear layers for this flow configuration. Meanwhile, the negative vorticity of the natural flow creates a favourable environment for the amplification of the negative sign vortex created by the ZNMF jet. This in turn results in the negative sign vortex being amplified to the point where it is observed to be two orders of magnitude larger than the characteristic dimension of the jet orifice; a size that is clearly large enough to affect the global airfoil flow field dynamics.

In describing the flow field around the controlled airfoil it is tempting to refer to it as being attached to the airfoil surface. Despite the fact that it is significantly more attached than the equivalent uncontrolled flow it must be noted that it is not fully attached, as at any point in time at least one recirculation region exists above the upper surface of the airfoil. It is the reduction of the massive recirculation region characteristic of the uncontrolled airfoil to a single, or a pair, of much smaller, controlled recirculation regions that results in the performance benefits noted for the controlled airfoil.

Three mechanisms through which the generated vortices affect reattachment of the flow field are proposed. Firstly, the addition of large-scale structures significantly enhances the entrainment of the shear layer. It is also postulated that the negatively rotating vortex transfers rotational momentum to the shear layer via viscous forces. Both of these mechanisms act to deflect the shear layer towards the airfoil surface. The final mechanism identified assists the reattached shear layer to remain attached for phase angles where no large-scale structure is resident over the forward portion of the airfoil; the presence of the vortex deflects streamlines away from the surface, which results in alleviation of the local upstream pressure gradient, thereby reducing the forces promoting boundary layer separation.

Conclusions

The optimum forcing frequencies for active flow control to be implemented using a wall-normal ZNMF jet located at the leading edge of a NACA 0015 airfoil were identified to be F^+ = 0.7 or F^+ = 1.3. When a forcing frequency of F^+ = 1.3 was employed the most effective jet momentum was found to be c_μ = 0.14% (*VR* = 0.65). Using these forcing parameters the airfoil stall angle was mitigated from $\alpha = 10^o$ to $\alpha = 18^o$, resulting in a maximum lift coefficient increase of 46% above the uncontrolled lift coefficient. Improvement of the lift-to-drag ratio was also noted throughout the range of post-stall angles of attack investigated. Activation of the control resulted in the flow over the suction surface of the airfoil being seemingly more attached for a wider range of angles of attack. The reattachment of the flow was attributed to the generation of a train of spanwise lifting vortices that appeared to roll down the upper surface of the airfoil. The lower effective forcing frequency was observed to result in a single vortex being present over the suction surface of the airfoil at any point in time, whereas the upper effective frequency resulted in two vortices residing over the airfoil surface throughout the excitation period. A number of potential mechanisms through which the spanwise vortices affected reattachment of the flow were identified.

References

[1] Chang, R., Hsiao, F. and Shyu, R., Forcing Level Effects of Internal Acoustic Excitation on the Improvement of Airfoil Performance, *Journal of Aircraft*, **29 (5)**, 1992, 823-829.

[2] Donovan, J., Kral, L. and Cary, A., *Active Flow Control Applied to an Airfoil*, AIAA Paper 98-0210, 1998.

[3] Lee, C., Ha, Q.P., Hong, G. and Mallinson, S., A piezoelectrically actuated micro synthetic jet for active flow control, *Sensors and Actuators* A 108, 2003, 168-174.

[4] Seifert, A., Bachar, T., Shepshelovich, M. and Wygnanski, I., Oscillatory Blowing: A Tool to delay Boundary Layer Separation, *AIAA Journal*, **31 (11)**, 1993, 2052-2060.

[5] Seifert, A., Darabi, A. and Wygnanski, I., Delay of Airfoil Stall by Periodic Excitation, *Journal of Aircraft*, **33 (4)**, 1996, 691-698.

[6] Seifert, A. and Pack, L., Active Flow Separation Control on Wall Mounted Hump at High Reynolds Numbers, *AIAA Journal*, **40 (7)**, 2002, 1363-1372.

[7] Smith, B and Glezer, A., The formation and Evolution of Synthetic Jets, *Physics of Fluids*, **10 (9)**, 1998, 2281-2297.

[8] Soria, J., An investigation of the near wake of a circular cylinder using a video-based digital cross-correlation particle image velocimetry technique, *Experimental Thermal Fluid Science*, 1996, **12**, 221-233.